Method of Moments Analysis of an Axisymmetric Chiral Radome

***Halid Mustacoglu*[1], *Joseph R. Mautz*[2], *and Ercument Arvas*[3]**

[1]Anaren Microwave, Inc., East Syracuse, NY 13057, hmustacoglu@anaren.com

[2]Syracuse University, Department of EECS, Syracuse, NY 13244, jrmautz@syr.edu

[3]Syracuse University, Department of EECS, Syracuse, NY 13244, earvas@syr.edu

Abstract

An axisymmetric chiral radome has been analyzed numerically by using the method of moments. The chiral body is illuminated by a plane wave and the surface equivalence principle is used to replace the body by equivalent electric and magnetic surface currents. The scattered field outside and the total internal field are produced by these equivalent currents. By using the boundary conditions on the surfaces of the body, eight simultaneous surface integral equations are obtained for four unknown equivalent surface currents. These eight equations are reduced to four by taking linear combinations of them. A Matlab computer program is developed for an axisymmetric chiral radome and examples of numerical calculations are given for a chiral spherical radome and chiral Von Karman radome. Numerical results of the chiral spherical radome are in excellent agreement with the exact ones obtained by the eigenfunction solution.

1. Introduction

A radome is a structure used to protect antennas from outside weather effects such as rain, snow, ice, etc. The construction materials of radomes are chosen such that the electromagnetic signal should be affected minimally. Several shapes of radomes with various materials are built where they can be seen used at many places like airplanes, on the ground covering various antennas, on boats and many more places.

Scattering and radiation from radomes and antenna systems with radomes have been studied in the last couple decades by using different methods, such as the ray tracing technique [1], the method of moments (MoM) [2], the physical optics (PO) method and dielectric physical optics (DPO) technique [3], the finite element method (FEM) [4], precorrected fast Fourier transform methods (P-FFT) [5], and body of revolution (BOR) formulations of MoM [6].

Chiral materials might be used to design anti-reflective structures to control scattering cross section patterns of bodies and scattering angles. We are not aware of any work that uses MoM to analyze an axisymmetric 3-D chiral radome to calculate the internal fields and scattering from it. In this paper, we present results for only two different shapes of axisymmetric chiral radomes.

2. Analysis

A chiral radome with 3 regions is shown in Fig. 1a. A body of revolution and the coordinate system are shown in Fig. 1b. The surface equivalence principle has been used to separate the radome problem into three parts, namely, the region external to surface 1, the region between surface 1 and surface 2, and the region bounded by surface 2. The radome is replaced by equivalent electric and magnetic surface currents, which produce the correct fields. The application of the boundary conditions on the tangential components of the total electric and total magnetic fields lead to coupled equations to be solved. Triangular expansion functions are used for both t-directed and Φ-directed currents. The coefficients that multiply these expansion functions are obtained using the method of moments.

978-1-4244-6051-9/11/$26.00 ©2011 IEEE

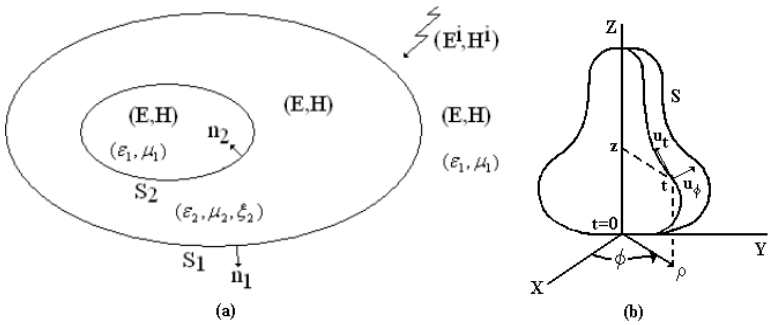

Fig. 1 a) An arbitrarily shaped chiral radome, b) A body of revolution and coordinate system

Using the equivalence principle, the original problem of Fig. 1a can be reduced to three simpler and equivalent problems shown in Fig. 2a, b, and c.

In the external equivalent problem, electric surface current $\mathbf{J}_1$ and magnetic surface current $\mathbf{M}_1$ have been placed on S_1. These surface currents are radiating in an unbounded medium of (ε_1, μ_1) with the same incident field of Fig. 1a. The total field at any point in the external region bounded by S_1 in Fig. 2a is the same as the total field at the same point of Fig. 1a, while the total field at any point in the internal region bounded by S_1 in Fig. 2a is zero. In other words,

$$\boldsymbol{E}_{1tan}(\boldsymbol{J}_1, \boldsymbol{M}_1) = -\boldsymbol{E}^i_{tan} \text{ on } S_1^- \tag{1}$$
$$\boldsymbol{H}_{1tan}(\boldsymbol{J}_1, \boldsymbol{M}_1) = -\boldsymbol{H}^i_{tan} \text{ on } S_1^- \tag{2}$$
$$\boldsymbol{J}_1 = \boldsymbol{n_1} \times \boldsymbol{H}^+_{\boldsymbol{out}} \tag{3}$$
$$\boldsymbol{M}_1 = \boldsymbol{E}^+_{\boldsymbol{out}} \times \boldsymbol{n_1} \tag{4}$$

where the superscript on S_1 denotes the surface just inside or outside S_1; "+" indicates the side of S_1 facing the region into which $\mathbf{n_1}$ points while "–" indicates the other side of S_1, and $\mathbf{E}_1(\mathbf{J}_1,\mathbf{M_1})$ and $\mathbf{H}_1(\mathbf{J}_1,\mathbf{M}_1)$, respectively, denote the electric and magnetic fields produced by the surface currents $\mathbf{J}_1$ and $\mathbf{M}_1$ when they radiate in the unbounded medium of (ε_1, μ_1). $\mathbf{n_1}$ denotes the unit outward vector on S_1 and ($\mathbf{E}_{out}^+$,$\mathbf{H}_{out}^+$) are the total fields just outside S_1 in Fig. 1a.

The fields internal to the chiral region can be found by using the equivalent problem shown in Fig. 2b. Here the surface currents $-\mathbf{J}_1$, $-\mathbf{J}_2$, $-\mathbf{M}_1$, and $-\mathbf{M}_2$ placed on S_1 and S_2 radiate in the unbounded medium of (ε_2, μ_2, ξ_2). They produce the correct total fields (**E**,**H**) at any point in the region bounded by S_1 and S_2 and produce zero fields at any point outside the region bounded by S_1 and S_2.

$$\boldsymbol{E}_{2tan}(\boldsymbol{J}_1, \boldsymbol{M}_1, \boldsymbol{J}_2, \boldsymbol{M}_2) = 0 \text{ on } S_1^+ \tag{5}$$
$$\boldsymbol{E}_{2tan}(\boldsymbol{J}_1, \boldsymbol{M}_1, \boldsymbol{J}_2, \boldsymbol{M}_2) = 0 \text{ on } S_2^+ \tag{6}$$
$$\boldsymbol{H}_{2tan}(\boldsymbol{J}_1, \boldsymbol{M}_1, \boldsymbol{J}_2, \boldsymbol{M}_2) = 0 \text{ on } S_1^+ \tag{7}$$
$$\boldsymbol{H}_{2tan}(\boldsymbol{J}_1, \boldsymbol{M}_1, \boldsymbol{J}_2, \boldsymbol{M}_2) = 0 \text{ on } S_2^+ \tag{8}$$
$$\boldsymbol{J}_2 = \boldsymbol{n_2} \times \boldsymbol{H}^-_{\boldsymbol{in}} \tag{9}$$
$$\boldsymbol{M}_2 = \boldsymbol{E}^-_{\boldsymbol{in}} \times \boldsymbol{n_2} \tag{10}$$

where S_1^+ and S_2^+ denote the sides of the surfaces S_1 and S_2 facing the regions into which the unit vectors $\mathbf{n_1}$ and $\mathbf{n_2}$ point, and $\mathbf{E}_2(\mathbf{J}_1,\mathbf{M_1}, \mathbf{J}_2,\mathbf{M_2})$ and $\mathbf{H}_2(\mathbf{J}_1,\mathbf{M_1}, \mathbf{J}_2,\mathbf{M_2})$, respectively, denote the electric and magnetic fields produced by the equivalent sources when they radiate in the unbounded medium of (ε_2, μ_2, ξ_2). $\mathbf{n_1}$ and $\mathbf{n_2}$ denote the unit vectors on S_1 and S_2, respectively and ($\mathbf{E}_{in}^-$,$\mathbf{H}_{in}^-$) are the total fields on S_2^- in Fig. 1a.

The fields in the region bounded by S_2 in Fig. 1a are found by using the equivalent problem shown in Fig. 2c. Here the surface currents $\mathbf{J}_2$, and $\mathbf{M_2}$ placed on S_2 radiate in the unbounded medium of (ε_1, μ_1). They produce the correct total fields (**E**,**H**) at any point in the region bounded by S_2 and produce zero fields outside the region bounded by S_2.

$$\boldsymbol{E}_{1tan}(\boldsymbol{J}_2, \boldsymbol{M}_2) = 0 \text{ on } S_2^- \tag{11}$$

$$\boldsymbol{H}_{1tan}(\boldsymbol{J}_2, \boldsymbol{M}_2) = 0 \text{ on } S_2^- \tag{12}$$

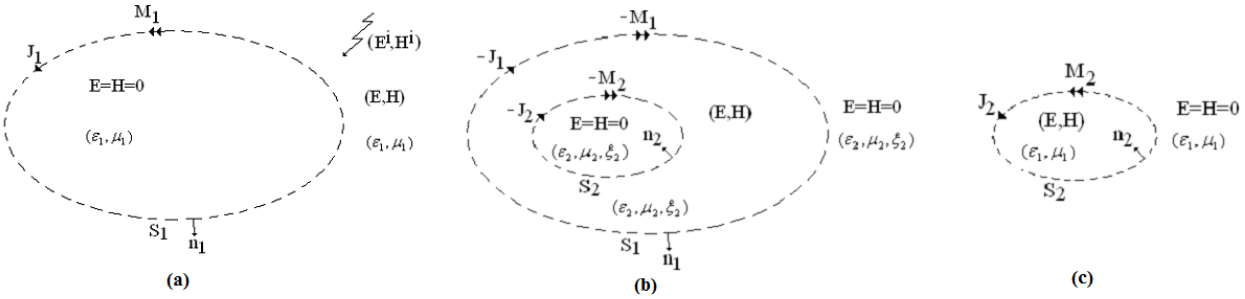

Fig. 2 a) External equivalence of the problem, b) Internal equivalence for the region bounded by S_1 and S_2, c) Internal equivalence for the region bounded by S_2

3. Formulation of Integral Equations

Equations (1), (2), (5) – (8), (11), and (12) represent eight coupled integral equations for the four unknown surface currents $\mathbf{J}_1$, $\mathbf{J}_2$, $\mathbf{M}_1$, and $\mathbf{M}_2$. The combined field formulation reduces these eight equations to four by adding (1) to (5), (6) to (11), (2) to (7) and (8) to (12). These four coupled integral equations are presented below. They are solved numerically by using the method of moments. The details of the solution procedure are available in [7].

$$-\boldsymbol{E}_{1tan}(\boldsymbol{J}_1, \boldsymbol{M}_1)|^{S_1^-} - \boldsymbol{E}_{2tan}(\boldsymbol{J}_1, \boldsymbol{M}_1, \boldsymbol{J}_2, \boldsymbol{M}_2)|^{S_1^+} = \boldsymbol{E}^i_{tan} \text{ on } S_1 \tag{13}$$

$$-\boldsymbol{E}_{1tan}(\boldsymbol{J}_2, \boldsymbol{M}_2)|^{S_2^-} - \boldsymbol{E}_{2tan}(\boldsymbol{J}_1, \boldsymbol{M}_1, \boldsymbol{J}_2, \boldsymbol{M}_2)|^{S_2^+} = 0 \text{ on } S_2 \tag{14}$$

$$-\boldsymbol{H}_{1tan}(\boldsymbol{J}_1, \boldsymbol{M}_1)|^{S_1^-} - \boldsymbol{H}_{2tan}(\boldsymbol{J}_1, \boldsymbol{M}_1, \boldsymbol{J}_2, \boldsymbol{M}_2)|^{S_1^+} = \boldsymbol{H}^i_{tan} \text{ on } S_1 \tag{15}$$

$$-\boldsymbol{H}_{1tan}(\boldsymbol{J}_2, \boldsymbol{M}_2)|^{S_2^-} - \boldsymbol{H}_{2tan}(\boldsymbol{J}_1, \boldsymbol{M}_1, \boldsymbol{J}_2, \boldsymbol{M}_2)|^{S_2^+} = 0 \text{ on } S_2 \tag{16}$$

4. Results and Conclusion

Numerical results for two chiral bodies, a spherical radome and a Von Karman radome are given in this paper. Figure 3 shows the radomes considered. The bodies are illuminated by a θ-polarized, z-travelling incident plane wave where its electric field is x-directed.

Internal fields on the z-axis and the scattering from the bodies have been computed. Results are given for a spherical radome of outer radius $10\lambda_0$ and inner radius $9.5\lambda_0$, $\varepsilon_r = 1.2$, $\mu_r = 1$, and $\xi_r = 0.2$ for $\theta^{inc} = 180°$ in Fig. 4, and in Fig. 5, results for a Von Karmon radome of $L1 = 10.1\lambda_0$, $L2 = 10\lambda_0$, $D1 = 1.1\lambda_0$, and $D2 = 1\lambda_0$ with $\varepsilon_r = 1.55$, $\mu_r = 1$, and $\xi_r = 0$, 0.3, 0.6, and 0.9 for $\theta^{inc} = 0°$ are given.

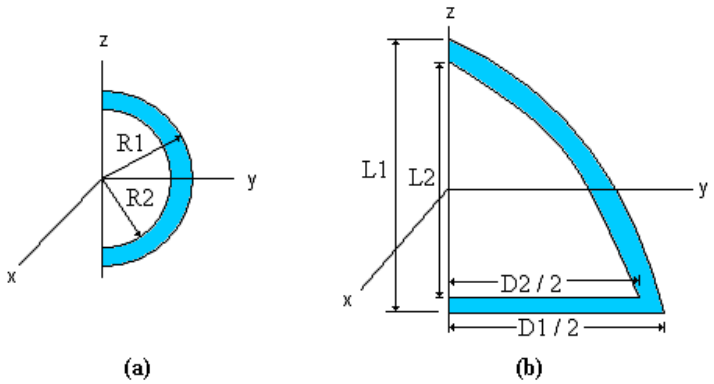

Fig. 3 a) Spherical radome, b) Von Karmon radome

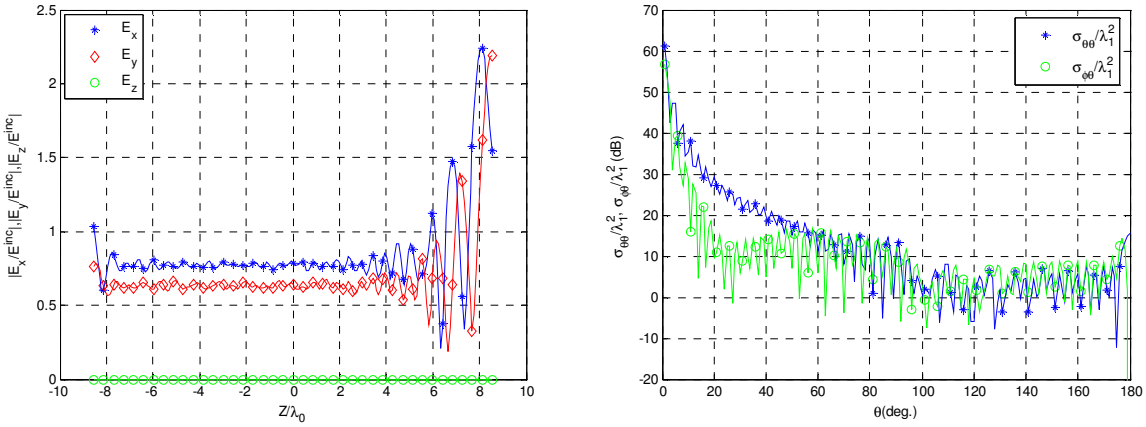

Fig. 4 Internal fields on the z-axis and scattering cross section of a spherical radome.

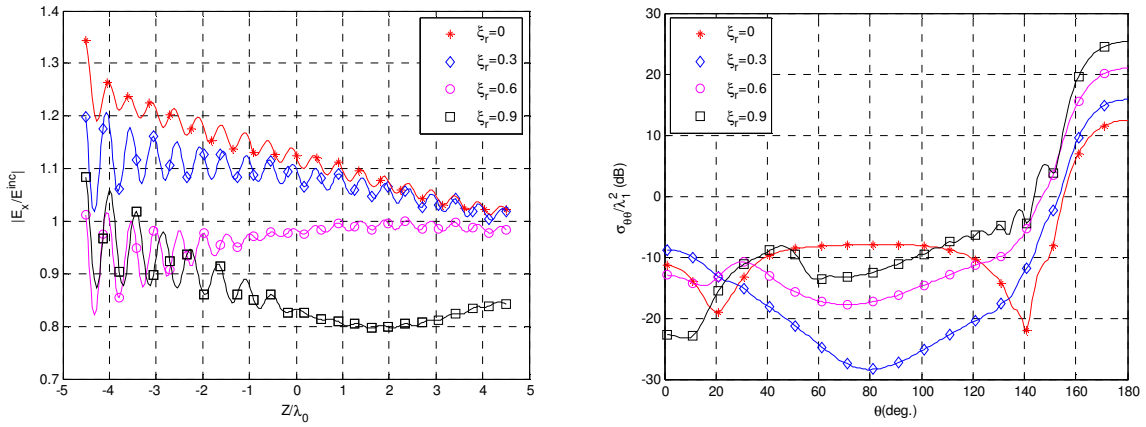

Fig. 5 Internal fields on the z-axis and scattering cross section of a Von Karmon radome.

Results of Fig. 4 are in excellent agreement with the exact data. It is observed that, adding chirality to the bodies caused the cross-polarized field component to evolve and the magnitude of the cross-polarized field component to shift the direction of the scattered fields away from the direction of the incident fields. Adding chirality to the bodies affected the inside fields and the scattered fields significantly for the cases studied in this paper.

5. References

1. D. T. Paris, “Computer-aided radome analysis,” *IEEE Trans. Antennas Propagat.*, vol. AP-18, Jan. 1970, pp. 7–15.
2. E. Arvas, S. Ponnapalli, “Scattering cross section of a small radome of arbitrary shape,” *IEEE Trans. Antennas Propagat.*, vol. 37, No. 5, May 1989, pp. 655–658.
3. R. E. Hodges and Y. Rahmat-Samii, “Evaluation of dielectric physical optics in electromagnetic scattering,” in *AP-S Int. Symp. Dig.,* Ann Arbor, MI, vol. 3, June 1993, pp. 1742–1745.
4. R. K. Gordon and R. Mittra, “Finite element analysis of axisymmetric radomes,” *IEEE Trans. Antennas Propagat.*, vol. 41, July 1993, pp. 975–981.
5. X. C. Nie, N. Yuan, L. W. Li, T. S. Yeo, Y. B. Gan, “Fast analysis of electromagnetic transmission through arbitrarily shaped airborne radomes using precorrected-FFT method,” *Progress In Electromagnetics Research, PIER.*, vol. 54, 2005, pp. 37–59.
6. J. R. Mautz, R. F. Harrington, “Radiation and scattering from bodies of revolution,” *Appl. Sci. Res.*, vol. 20, No. 6, June 1969, pp. 405–435.
7. H. Mustacoglu, "MoM Analysis of an Axisymmetric Chiral Radome," PhD. Dissertation, Syracuse University, December 2010.